AIAA JOURNAL
Vol. 36, No. 6, June 1998

Passive Control of Pressure Fluctuations Generated by Separated Flow

A. F. Heenan* and J. F. Morrison†
Imperial College, London SW7 2BY, England, United Kingdom

Measurements of wall-pressure fluctuations have been made in the flow behind a backward-facing step, with a permeable reattachment surface. Different configurations are tried, the most successful producing a reduction in peak rms pressure fluctuation of about 13% and a reduction in drag of about 9%. Spectra show that most of the attenuation occurs at low frequencies, and in particular, the "flapping" frequency ($n \approx 0.1$) is effectively removed. The main reason for this appears to be that the permeable surface inhibits the upstream convection of disturbances produced at reattachment. Structural modifications to the pressure-fluctuation field appear to be confined to the region upstream of mean reattachment.

Nomenclature

C_p	= coefficient of static pressure
f	= frequency
g	= function
h	= step height
n	= dimensionless frequency, fx_R/U_e
p	= wall pressure
q	= freestream dynamic head
Re_h	= Reynolds number, based on step height
$U, V, W,$ u, v, w	= mean and fluctuating components of velocity in mutually orthogonal directions; x, y, z directions, respectively
x	= streamwise direction, parallel with wall
y	= wall-normal direction
θ	= momentum thickness
$\theta(f)$	= phase angle
φ	= wall-pressure spectrum function
ψ	= wavelet function

Superscripts and Subscripts

e	= freestream or at separation
h	= step height
p	= propagation
R	= reattachment

Introduction

BUFFET onset usually coincides with the first local occurrence of incipient separation, and the severity of buffet excitation (and therefore buffeting, the structural response) depends on the development of the separated region. The alleviation of buffet by passive means is highly desirable because of the expected increase in the lifetime of wing components. This problem relates to a variety of flow types,[1] all with the characteristics of a separation followed by a curved mixing layer with subsequent reattachment. In the present experiment, the flow over a backward-facing step (backstep) is used to create a well-defined, large separation, which is typical of those found on aircraft and which allows the important physical processes to be studied without ambiguity.

Reattachment on an impermeable surface has been documented in detail by Wood and Bradshaw,[2] who show that the impermeability constraint, which affects eddies out to a distance from the wall of the same order as their wavelength, produces an initial rise in the wall-normal Reynolds stress $\overline{v^2}$ across the whole layer. This is opposite to what might be expected intuitively, although farther downstream it decreases in conformity with the impermeability constraint. The effect of the wall on the pressure field and, in particular, the modification of the pressure-strain terms are responsible for this initial rise, which can be explained by the effect of the instantaneous mirror image of the reattaching structure. Thus, in the present work, the surface in the reattachment region is replaced by a permeable one. This weakening of the impermeability constraint is expected to modify pressure disturbances via the pressure-strain terms, thereby reducing $\overline{v^2}$, which is otherwise not brought to zero at the wall. The effect of the impermeability constraint on the v-component motion can also be associated with the generation of pressure fluctuations via the source terms in the Poisson equation for pressure fluctuations, which for a thin shear layer is

$$-\nabla^2 \frac{p}{\rho} = 2\frac{\partial U}{\partial y}\frac{\partial v}{\partial x} + \frac{\partial^2}{\partial x \partial y}[uv - \overline{uv}] \tag{1}$$

Using a direct-numerical simulation database, Kim[3] assessed the relative contributions of the rapid and slow source terms for channel flow: for the wall pressure, they are of similar magnitude, whereas in midchannel, most of the rapid pressure resides at low wave numbers. Thus, for the present configuration, it seems reasonable to assume that near the position of maximum rms pressure fluctuation, which lies upstream of the mean reattachment position x_R, contributions from the rapid term will dominate. This is because large eddies upstream of x_R, which experience the effect of the impermeability constraint first, reattach, producing low-wave-number pressure fluctuations, whereas downstream of x_R, smaller eddies produce pressure fluctuations of higher wave number on reattaching. The wall-pressure spectra of Farabee and Casarella[4] broaden as the position of measurement moves downstream through x_R.

Particularly at small distances from the step, wall-pressure spectra are dominated by contributions from the phenomenon known as flapping (a low-frequency unsteadiness), which occurs at frequencies $n = fx_R/U_e \approx 0.1$, that is, at frequencies about six to eight times[5] less than those associated with the largest structures in the mixing layer. Flapping has been demonstrated by a number of authors in a number of configurations including that of a backstep.[6–10] Cherry et al.,[7] using a blunt leading-edge geometry, attributed flapping to the shedding of vorticity from the recirculating region and suggested that it was indicative of a growth–decay cycle of the bubble. It has also been observed using a flat plate, normal to the flow, with a splitter plate by Castro and Haque[9] and in backstep flow by Eaton and Johnston,[8] who suggested that the cause was an instantaneous imbalance between entrainment of fluid by the mixing layer from the recirculation region and that reinjected near reattachment. Kiya and Sasaki[10] also observed flapping of a separated shear layer from a blunt leading edge, and they also attributed this to the shedding of vorticity accumulated in the bubble. Subsequently, Kiya and Sasaki[11] suggested that flapping was caused

Received Nov. 4, 1995; presented as Paper 96-0445 at the AIAA 34th Aerospace Sciences Meeting, Reno, NV, Jan. 15–18, 1996; accepted for publication Jan. 19, 1998.

*Graduate Research Assistant, Department of Aeronautics.
†Senior Lecturer, Department of Aeronautics.

by a short-term breakdown in the spanwise coherence of the large, hairpin-shape eddies, thereby reducing the rate of entrainment by the mixing layer from the recirculating region, thus leading to a buildup of fluid within it and its subsequent sudden release. Several authors have suggested that flapping is the result of a feedback mechanism, where disturbances generated at reattachment are fed back upstream into the separating shear layer.[1,9]

On the other hand, some authors have not observed flapping either in a backstep flow[12] or in flow over a bluff plate with a long splitter plate.[13] Among workers who have observed the phenomenon, there is yet no full agreement on its precise nature, let alone its cause. However, existing theories usually involve the imbalance between mass flux out of the bubble by entrainment and that fed back upstream from reattachment. Bradshaw and Wong[14] suggest that the large eddies are torn in two at reattachment, whereas other authors suggest that the large eddies pass upstream and downstream more or less alternately: This may provide a clue to the possible source of the unsteadiness. Eaton and Johnston[8] used wall thermal tufts to show that the unsteadiness causes the short-time-averaged reattachment point to oscillate by about two step heights about the mean reattachment point. Driver et al.[6] show, also through the use of conditional sampling, that the entire recirculation region oscillates, yet with streamlines remaining closed at the extremes of the cycle.

Eaton and Johnston[8] suggest that flapping may be related to the low-frequency unsteadiness observed in free-shear layers with large impingement angles.[15] However, Rockwell and Naudascher[16] note that, in the case of extremely small impingement angles as in the present case, the oscillations are not related to those produced by edge, ring, or shear tones. Moreover, flapping occurs at frequencies that are typically one order of magnitude lower than those produced by impingement, and yet large, low-frequency oscillations of a separated shear layer, in which the turbulent pressure fluctuations are already large, are likely to have a major effect on the response of the adjacent structure. Not only does the present work demonstrate a means of attenuating these low frequencies, but it also shows how the recirculating region may be steadied by passive mass transfer through a permeable reattachment surface.

Apparatus

Figure 1 is a schematic of the test rig that is placed in a recirculating wind tunnel of 914 × 914 mm cross section, chosen especially for its quietness and low vibration. The freestream turbulence intensity of the tunnel is less than 0.05%. The part of the model upstream of the backstep was derived from an Eppler 334 airfoil section, chosen because of its flat pressure surface. The section was truncated at the point where the suction surface is parallel to the pressure surface, and these continue parallel to each other up to the top of the step. The model is placed at a small, negative, angle of attack such that the pressure gradient along the pressure surface of the model is approximately zero. This angle of negative incidence (≈3.0 deg) corresponds roughly to the zero-lift angle of the Eppler section.

The aspect ratio (tunnel width/step height) is 12 so that three-dimensional effects along the model centerline are avoided, according to the criterion established by de Brederode and Bradshaw.[17] The trailing edge of the model was streamlined to minimize any wake-induced unsteadiness. Table 1 summarizes the experimental conditions. The geometric expansion ratio (ER) at the backstep is slightly reduced if allowance is made for viscous blockage: The backstep causes a 5.5% decrease in measured freestream velocity.

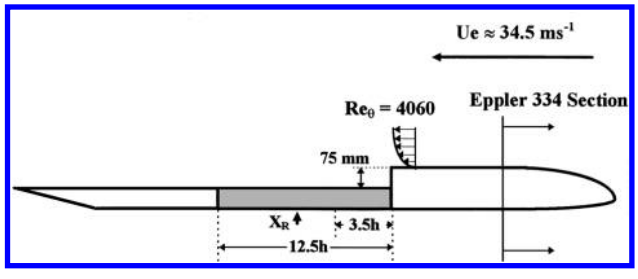

Fig. 1 Rig schematic. Surface geometry: permeable configuration; 0–3.5*h* and 0–12.5*h*; OAR, 5, 20, and 50%.

Table 1 Experimental conditions

U_e	$Re_{\theta e}$	Re_h	ER	h/δ_e	AR
34.5 ms^{-1}	4060	1.9×10^5	1.1	4.7	12.2

The ratio of step height h to boundary-layer thickness at separation, δ_e, is about 3.1, which represents a large perturbation compared with the values of h/δ_e used by other workers.[14] No attempt was made to dissociate the effects of the change in flow species at separation from those at reattachment, as done by Chandrsuda and Bradshaw,[12] the particular objective of this experiment being to generate a large, well-defined separation. The permeable reattachment surface consists of a regular array of circular holes. Beneath the permeable surface, there is an acoustically untuned chamber, which extends the full length of the permeable surface. It is nominally airtight so that the net mass flux through the permeable plate at any time is zero.

Wall-pressure fluctuations have been measured for a range of open-area ratios (OAR) extending from 5 to 50% and for a number of configurations: In the present work, results for a permeable surface extending from the foot of the backstep to 3.5*h* and 12.5*h* downstream are compared with the impermeable geometry. The 0–3.5*h* configuration was chosen because, in this case, the permeable surface would be expected to affect only the recirculation region, the local streamwise velocity over the permeable surface being toward the step for nearly all of the time, whereas in the 0–12.5*h* configuration, the instantaneous reattachment point would be expected to be upstream of the permeable/impermeable surface change for most of the time.[8]

The flush-mounted pressure transducers are 0–0.138 Nm^{-2} in range and consist of a diaphragm on which is diffused a semiconductor Wheatstone bridge: The external diameter is 2.3 mm, although allowance for an inflexible rim would reduce the effective size. The resonant frequency is about 45 kHz. Purpose-built circuits were designed to drive and amplify the signal output: The gain–bandwidth product of the amplifier is about 6×10^6, the frequency response being virtually flat up to about 30 kHz for a gain of about 100. The transducers and their analog circuitry are of the same make and design as used successfully by Morrison and Bradshaw[18] for the investigation of pressure fluctuations in boundary layers.

Analysis

The spectra are plotted in the form appropriate for buffet studies as suggested by Owen,[19] that is, $\sqrt{[n\phi(n)]}$ against n, where

$$\frac{\overline{p^2}}{q^2} = \int_0^\infty \phi(n)\,\mathrm{d}n = \int_0^\infty n\phi(n)\,\mathrm{d}(\log n) \qquad (2)$$

where q is the freestream dynamic head. Owen shows that, assuming that the structural response has a narrow acceptance band that is independent of the aerodynamic conditions, the rms intensity of the aerodynamic excitation is proportional to $\sqrt{[n\phi(n)]}$. Equation (2) shows that the area under the spectra on linear/log axes is proportional to the square of the ratio of the energy of the excitation to the freestream dynamic head. It is also interesting to note that, for $\phi(n)$ as it is defined in Eq. (2), $n\sqrt{[n\phi(n)]}$ is equivalent to a spectrum of pressure-gradient fluctuations because differentiation corresponds to multiplication of the spectrum by frequency. Mabey[1] has shown that spectra, in this form, are similar for a wide range of bubbles.

Particular care was taken to ensure that the data were free from extraneous influences such as vibration, acoustic resonances, or diffuser-induced disturbances. Initially, a Wiener filter was used with the method of Horne and Handler[20] to deduce the form of the filter function, which can be obtained from phase information between two transducers separated in the spanwise (homogeneous) direction. The fundamental organ-pipe resonance occurs at about 34 Hz: Many of the higher harmonics are also identifiable, as are the blade-passing frequency (~315 Hz) and frequency of the power supply (50 Hz). Because the maximum attenuation of the filter at any frequency appears to be about 0.5 dB only, in a signal that extends over a range of 60 dB, the data were subsequently analyzed without filtering, except

where measurements were taken very close to the step, where rms levels are quite low so that filtering then became necessary.

Results

Table 2 shows model drag coefficients at the operating condition, estimated by integration of the momentum deficit of the model wake. The drag is progressively reduced as the OAR increases, although, interestingly, the 0–3.5h configuration is considerably more effective in reducing the drag than the 0–12.5h one. The 50% OAR, 0–3.5h configuration provides a 9% reduction in drag.

Table 3 shows, for the three configurations, reattachment lengths measured by two different techniques. For the impermeable case, chalk/paraffin flow visualization showed this to be 6.25h. The mean skin friction downstream of the step in the case of the impermeable and 0–3.5h configurations was also determined by a sublayer-fence probe, which gave very similar results. For all three configurations, wool tufts were also used, and they gave qualitative agreement.

Figure 2 shows the corresponding mean static pressure distributions. In Fig. 3, the variation of rms pressure fluctuation through reattachment is compared, for the impermeable case, with data from Farabee and Casarella[4] and data from a simulation by Le and Moin.[21] Differences appear to be due to the differences in Reynolds number and, in particular, the ratio h/δ_e: In the present case, this ratio is about seven times that of Driver et al.[6] In each case, it is clear that the maximum occurs about one step height upstream of x_R, and use of these maxima to infer an estimate for x_R gives values that compare well with the measured estimates of x_R in Table 3. The split-film estimates of x_R are used to nondimensionalize the frequency of the pressure-fluctuation data.

Table 2 Drag coefficients

Configuration	0%	5%	20%	50%
Impermeable	0.152	——	——	——
0–3.5h	——	0.148	0.142	0.139
0–12.5h	——	0.152	0.145	0.145

Table 3 Mean reattachment lengths, x_R

Configuration	Sublayer-fence probe	Chalk/paraffin	Split-film probe
Impermeable	5.5h	6.25h	5.5h
0–3.5h	6.0h	——	5.75h
0–12.5h	7.0h	——	7.00h

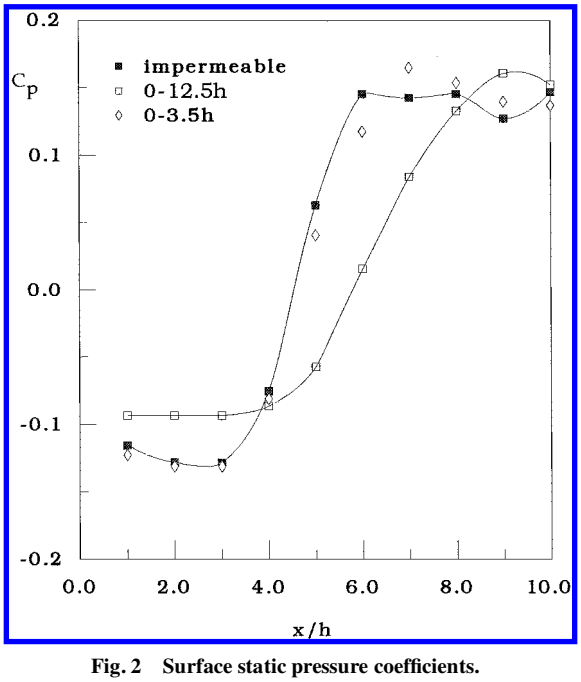

Fig. 2 Surface static pressure coefficients.

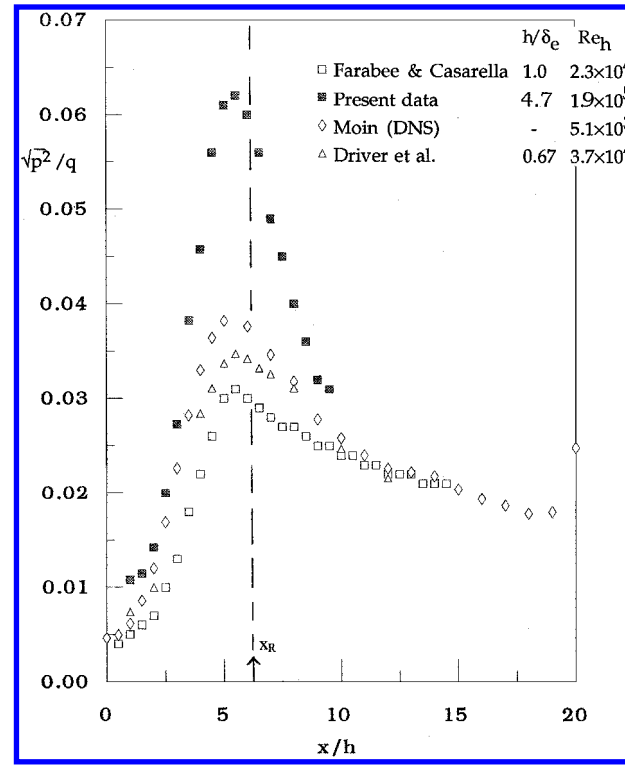

Fig. 3 Impermeable surface, rms of surface pressure fluctuations.

Figure 4 shows rms pressure distributions for each of the configurations tested: As the OAR is increased, the rms pressure up to x_R is progressively attenuated, the 0–12.5h configuration providing the greatest attenuation up to that point. What happens downstream of x_R depends on the extent of the permeable surface, which increases the rms pressure. This is probably because the linear source term in Eq. (1) is nonzero at the permeable surface, which is also likely to increase the turbulent stresses adjacent to it. In general, the wall-pressure fluctuations will increase with the Reynolds stresses. In each case where the peak rms pressure is reduced, it also moves downstream. This is in common with a number of experiments on impermeable surfaces; where the turbulence intensity is reduced overall, x_R increases.

The wall-pressure spectra for the impermeable surface, plotted in the form given by Eq. (2), are compared with those for the 0–3.5h and 0–12.5h configurations in Figs. 5 and 6, respectively. The OAR is 20% in both cases. The area under the spectra integrates to the square of the rms values in Fig. 4b. Following the suggestion of Mabey,[1] the spectra are compared at the same position as a fraction of bubble length, x/x_R: The justification for this normalization appears in Figs. 5e and 6d, which both show that the spectra collapse on U_e and x_R downstream of reattachment. For the impermeable surface, the flapping frequency is identifiable in Fig. 5 at $n \approx 0.1$, and this secondary peak (or plateau) appears to reach a maximum near $x/x_R = 0.75$ ($x = 4.5h$), the position of maximum pressure recovery in the bubble (Fig. 2). This peak, and in fact all of the lower-frequency energy, is attenuated by both of the permeable configurations at all positions up to x_R, the attenuation being the greater for the 0–12.5h case. For the 0–3.5h configuration, there is attenuation downstream of the end of the permeable surface: This is likely to be because the pressure fluctuations are convected in the mixing layer beyond the region in which attenuation is effective.

The large-eddy peak at $n \approx 1.0$ appears to be attenuated by the presence of the permeable surface as well. The greatest degree of attenuation of this peak occurs at $x/x_R = 1.0$ for the 0–12.5h case (Fig. 5d) and $x/x_R = 0.5$ for the 0–3.5h case (Fig. 6a). In both cases, eddies that reattach at these streamwise locations do so on a permeable part of the surface. (There is no corresponding attenuation at $x/x_R = 1.0$ for the 0–3.5h case.) The effect is interesting in that it must be the result of the way in which the wall modifies pressure disturbances as opposed to the diminution of the rapid source term in Eq. (1), which can increase only on a surface on which the

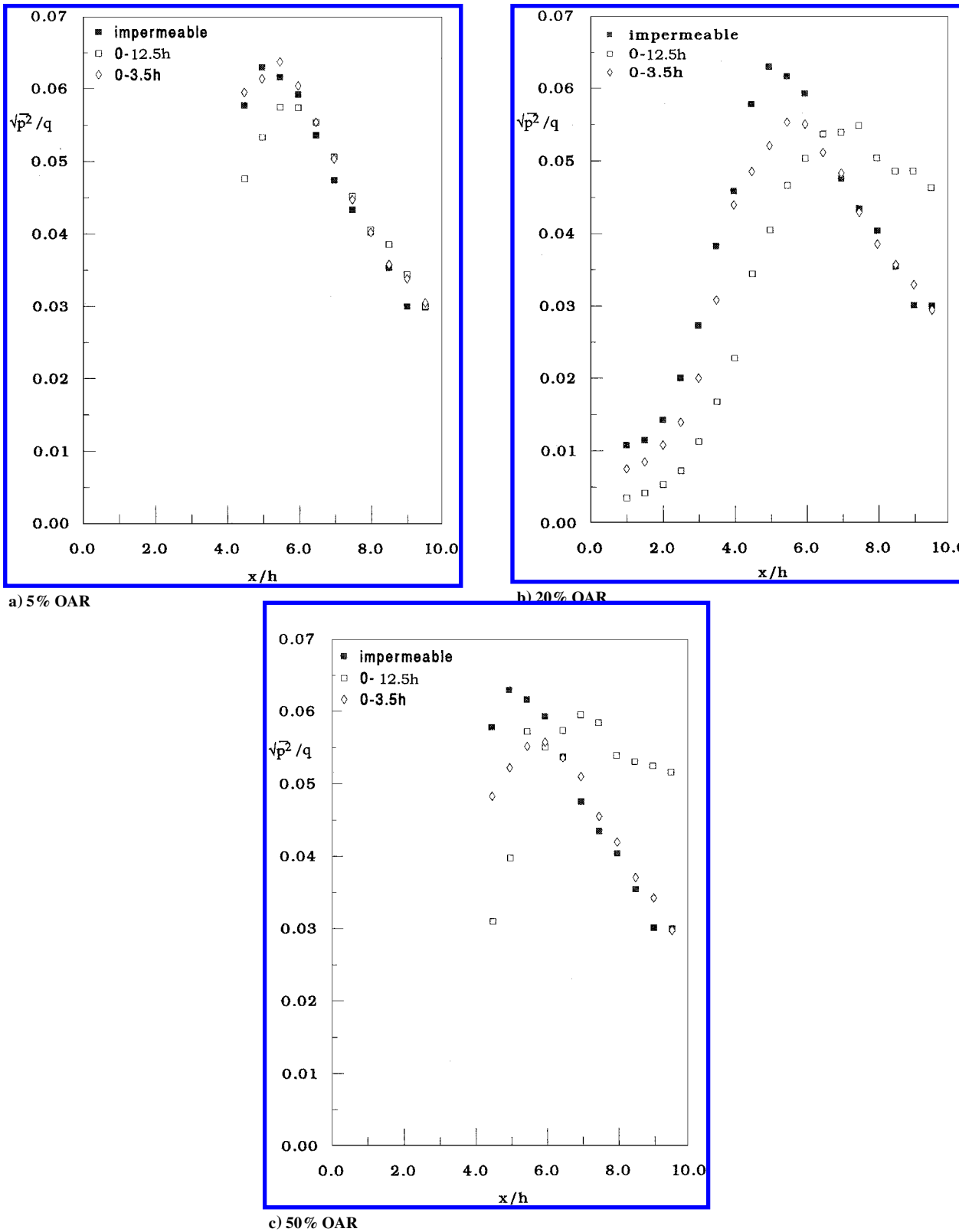

a) 5% OAR

b) 20% OAR

c) 50% OAR

Fig. 4 RMS pressure.

impermeability constraint is not enforced. It is likely that the rapid term would be the dominant one of the two source terms at these positions immediately upstream of reattachment where the large eddies resemble most those found in turbulent channel flow in which most of the rapid pressure resides at low wave numbers.[3] This only serves to emphasize the differences between the way in which the wall modifies pressure disturbances in the impermeable case and the way it does so when permeable: Wood and Bradshaw[2] suggest that this process occurs as the instantaneous mirror image of the reattaching structures becomes important.

At higher frequencies ($n > 2$), the pressure fluctuations are also attenuated in the 0–12.5h configuration but not in the 0–3.5h one. This attenuation appears to be the greatest for $x/x_R = 0.5$, and by $x/x_R = 1.0$, any attenuation has disappeared. It is related to the modification of the pressure fluctuations in the mixing layer, either by the way in which pressure disturbances are modified by the adjacent permeable surface or by the way in which the source terms in Eq. (1) are affected by the permeable surface. It is related to the overall attenuation of the velocity field by the permeable surface and awaits further investigation. The spectra at $x/x_R = 1.0$ both

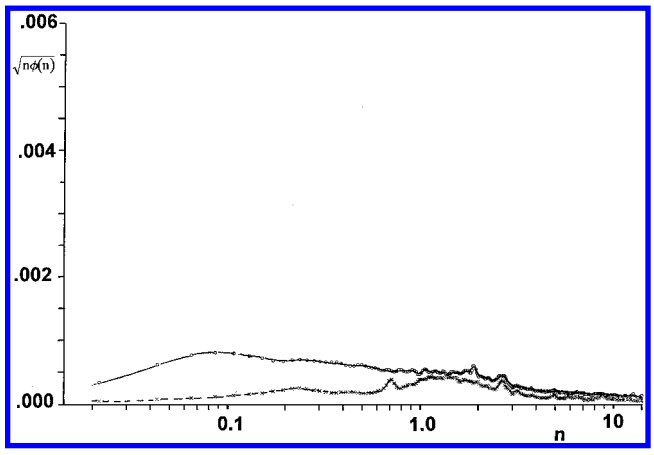

a) $x/x_R = 0.25$

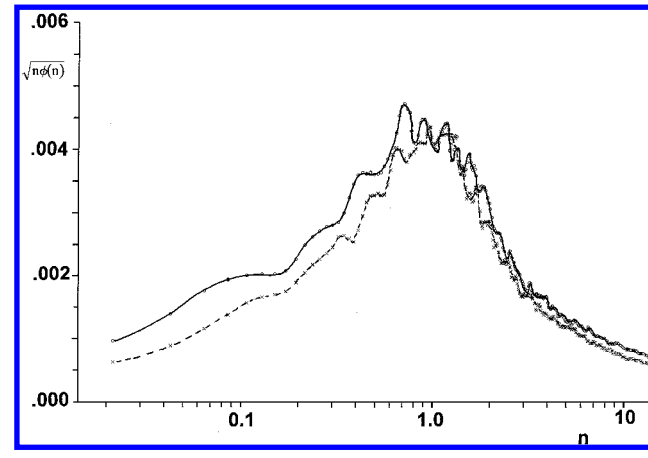

c) $x/x_R = 0.75$

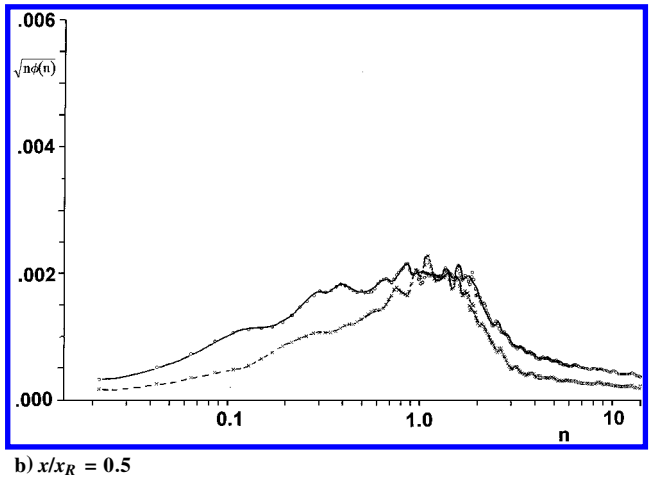

b) $x/x_R = 0.5$

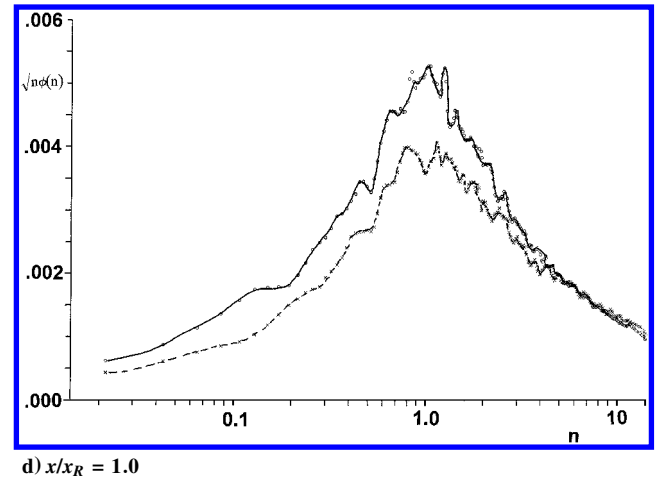

d) $x/x_R = 1.0$

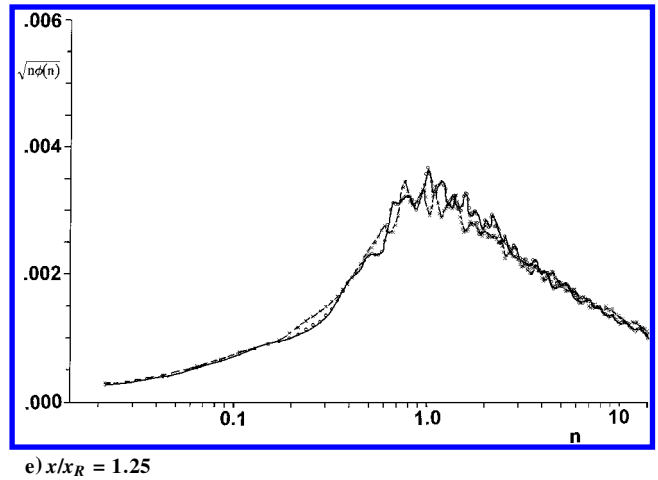

e) $x/x_R = 1.25$

Fig. 5 Wall pressure spectra, $\sqrt{[n\phi(n)]}$: ∘, impermeable, and ×, 0–12.5h.

asymptote to roughly the same levels at the high-frequency end, implying that the basic generation mechanisms for the high-frequency motion are the same on both the impermeable and permeable surfaces.

Independent measurements were made with two pressure transducers at each location to estimate the uncertainty of the wall-pressure data, which is typically 5% rms. The wake momentum measurements were performed several times to check repeatability. The drag coefficients were found to be repeatable to within 2% (95% confidence) once the variation in air density during a traverse had been minimized by running the tunnel for an hour before recording data.

Discussion

Because the spectral peaks in $\sqrt{[n\phi(n)]}$ roughly correspond to peaks in pressure-gradient fluctuations, $n\sqrt{[n\phi(n)]}$, the dominance of the flapping peak at $x/x_R = 0.75$ (Fig. 5c) and its coincidence with the position of maximum pressure recovery in the bubble (impermeable, $x/h \simeq 4.5$; 0–12.5h, $x/h \simeq 5.5$; Fig. 2) confirm that flapping is a genuinely unsteady phenomenon involving the whole bubble. A number of workers have identified the large-scale velocity fluctuations in the near-wall region to be driven by fluctuations in the streamwise pressure gradient.[5,22] On the impermeable surface, the peak rms pressure fluctuation is approximately 0.75h downstream of the location of the flapping peak.

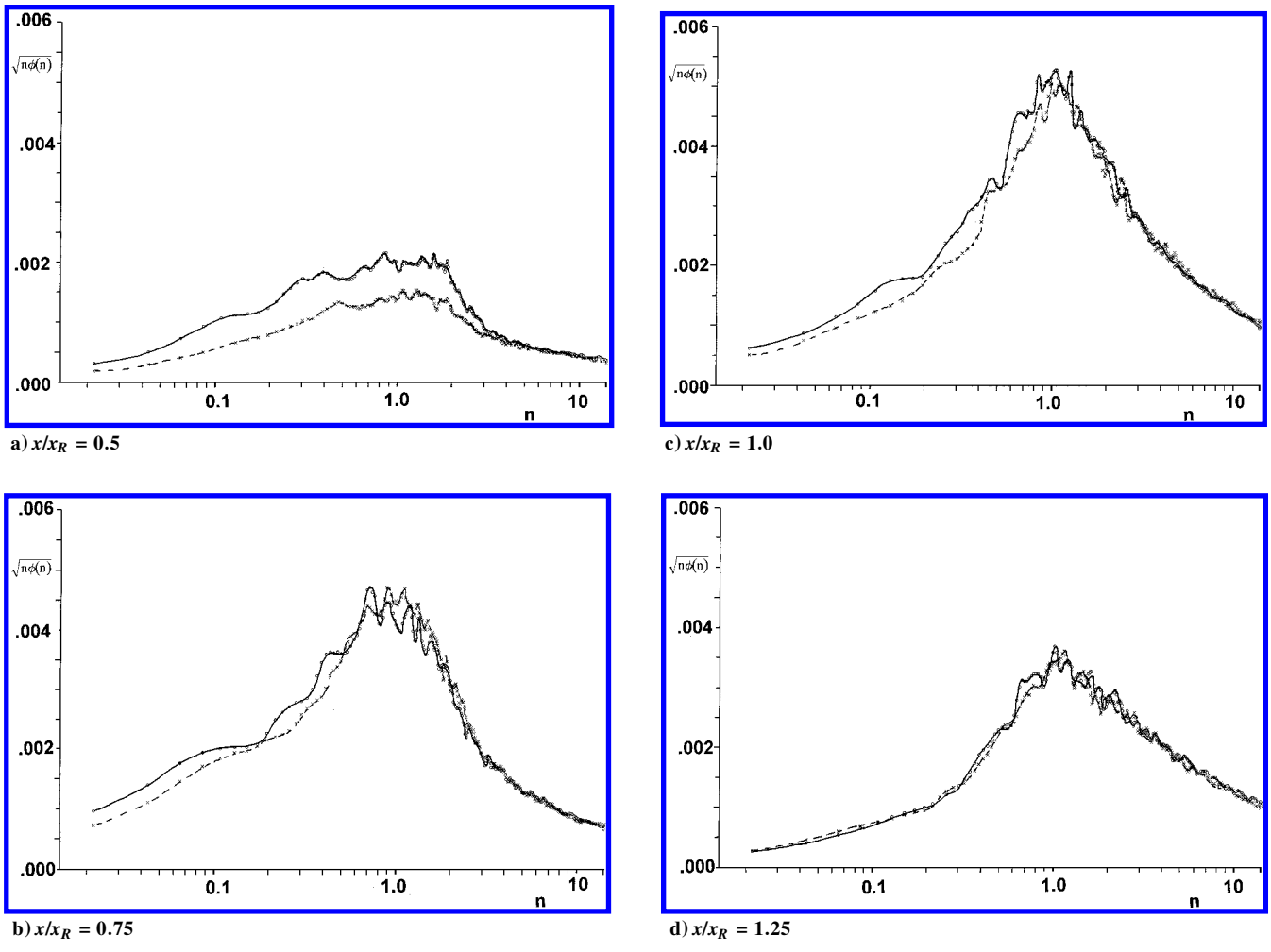

a) $x/x_R = 0.5$ c) $x/x_R = 1.0$

b) $x/x_R = 0.75$ d) $x/x_R = 1.25$

Fig. 6 Wall pressure spectra, $\sqrt{[n\phi(n)]}$: ∘, impermeable, and ×, 0–3.5h.

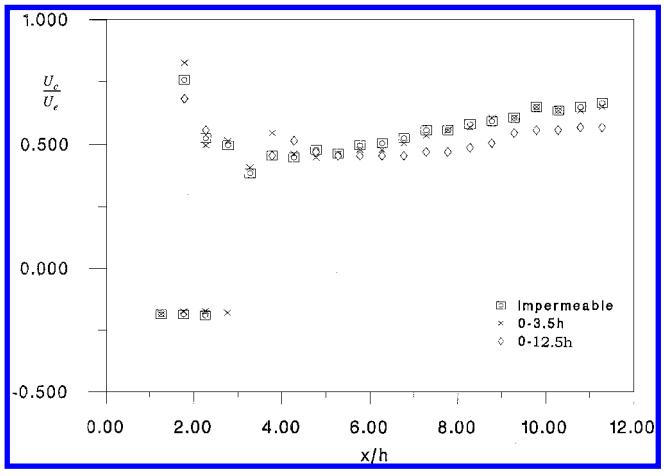

Fig. 7 Convection velocities of wall pressure from two transducers with separation $\delta x/h = 0.5$.

Figure 7 shows convection velocities as deduced from wall-pressure space–time correlations, with a fixed streamwise separation of 0.5h. Strictly, pressure fluctuations propagate as waves so that a propagation velocity is the correct term. However, much of the literature uses the term convection velocity so that both are used interchangeably here. For the impermeable configuration, at $x > 2.5h$ approximately, the determination of convection velocity is unambiguous. However, nearer to the step, a secondary peak appears in the correlation, which indicates upstream convection of pressure fluctuations. This secondary peak is not apparent for the 0–12.5h configuration, except possibly for those data taken nearest the backstep. The convection velocities appear to reach a minimum (positive) value near the position of maximum pressure recovery in the bubble (Fig. 2). The same data were also used to calculate cross spectra, for which the phase angles are shown in Fig. 8. The propagation velocity can be defined by

$$U_p = \frac{2\pi f\,\delta x}{\theta(f)} \tag{3}$$

where $\theta(f)$ is the phase angle. Thus, a negative propagation velocity is indicated by a negative phase angle, which is not plotted to avoid singularities. For the impermeable configuration, upstream convection is again apparent when $n < 1$ and $x/x_R < 0.4$ ($x/h < 2.5h$), approximately. For $x/x_R > 0.4$, there are no negative phase angles at low frequencies in the impermeable case. The crossover from positive to negative convection velocities occurs close to the spectral peak associated with the large eddies at $n \approx 1$, and the positive phase velocities are concentrated at frequencies that are about 10 times the flapping frequency. The effect of the permeable surface (0–12.5h) is to remove this upstream convection. The 0–3.5h configuration appears to do this, too, but more effectively,[23] given that the permeable surface is much shorter. However, Farabee and Casarella[4] show that, with an impermeable reattachment surface, long-time-averaged convection velocities are always positive and increase with frequency.

It seems that the 0–12.5h configuration does provide additional mass flux into the recirculation region at a fairly steady rate, relieving the static pressure not only so that the bubble is elongated in the streamwise direction but also so that upstream convection of fluid above the surface is not required to match the fluid entrained from the bubble by the mixing layer. This, therefore, provides a possible mechanism whereby the unsteadiness of the bubble is removed, the feedback process being attenuated or even removed. Confirmation of the reduced upstream convection caused by the

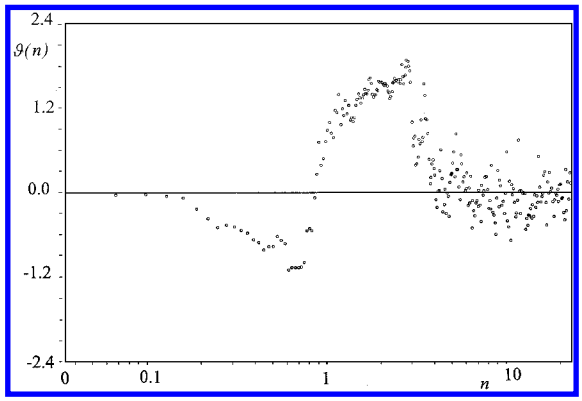

Impermeable

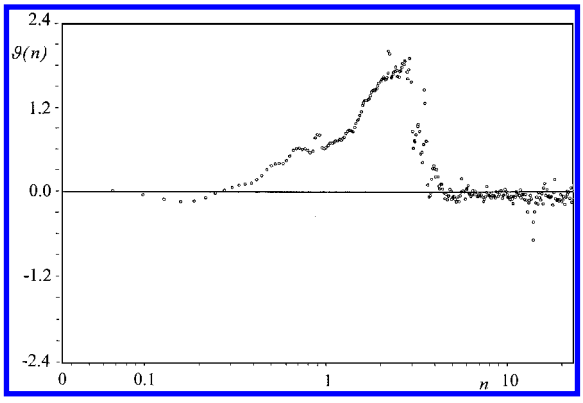

0–12.5*h*

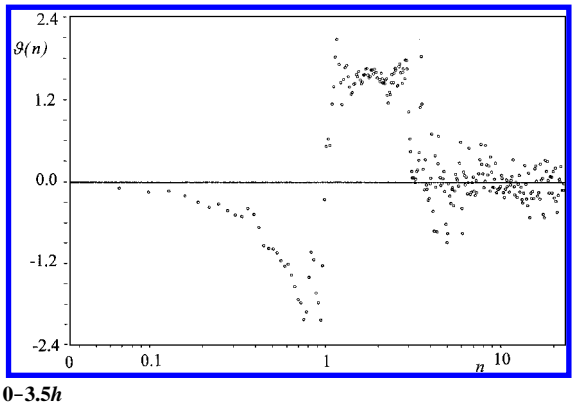

0–3.5*h*

Fig. 8 Phase angles from cross-power spectra of wall pressure from two transducers with separation $\delta x/h = 0.5$ at $x/x_R = 0.25$.

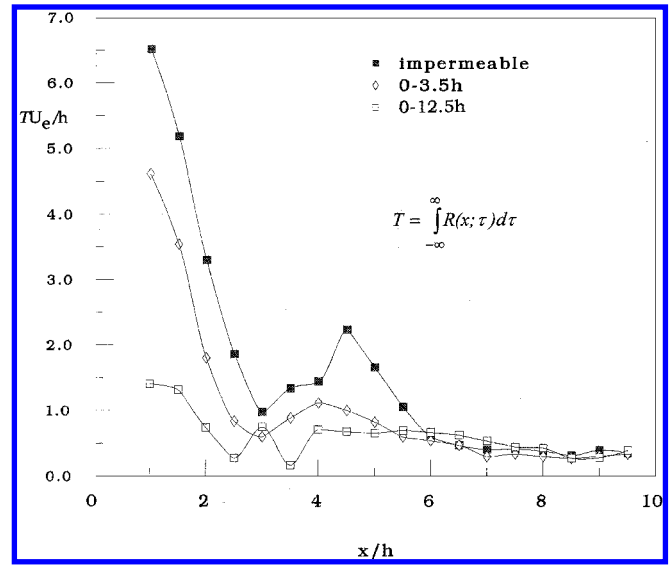

Fig. 9 Autocorrelation length scales.

permeable surface comes from flow visualization using wool tufts and is investigated further using triple split-film probes.[23] Further evidence for this modification of feedback comes from the attenuation of the higher-frequency pressure field at small distances from the step (Figs. 5a–5c). It suggests either that the permeable surface is more effective when upstream of x_R, presumably attenuating the pressure fluctuations in the free shear layer, or alternatively, the effect of the permeable surface is to impede the upstream convection of high-frequency pressure fluctuations from the point where they are produced farther downstream. However, the phase angles of Fig. 8 suggest that only low-frequency fluctuations are propagated upstream. This effect is currently being investigated in more detail, with particular reference to instantaneous flow reversals of the streamwise velocity.

Figure 9 shows streamwise correlation length scales of the wall pressure calculated from the integral of the autocorrelation at each point and using an estimated average convection velocity equal to U_e. The data of Fig. 7 show that the convection velocity is less than U_e and decreases to a positive minimum near $x/h = 4.5$. For $x/h < 4$, the convection velocity for the large-scale motion is small and negative. Therefore, for the impermeable-surface data, the length scales are overestimated in this region. However, it is worth remembering that integration of the autocorrelation for small distances from the step in the impermeable configuration will involve two peaks: the main one caused by the convection of the mixing layer and the other caused by the upstream propagation of pressure fluctuations. The absence of the latter in the 0–12.5h configuration is the main reason for the large drop in length scale near the step. In the impermeable configuration, the peak at $x/h \approx 4.5$ appears to be genuine and directly related to the flapping, which is most prevalent at this position (Fig. 5c).

The wavelet-coefficient contour plots (Fig. 10) were generated from u-component velocity time histories measured at $x/h = 1.0$ and $y/h = 0.0$ and at $x/h = 1.0$ and $y/h = -0.9$, where $y = 0$ corresponds to the height of the step. Triple-split, hot-film probes were used to obtain the two-dimensional, bidirectional data. Details of this probe, together with a complete assessment of the accuracy of the data, are given by Heenan and Morrison[24]; Daubechies[25] provides a full description of the wavelet technique. Briefly, in one dimension, the wavelet coefficients are defined by

$$\tilde{f}(\lambda, t_0) = \lambda^{-(1/r)} \int_{-\infty}^{\infty} g(t)\psi^* \left\{ \frac{(t - t_0)}{\lambda} \right\} \mathrm{d}t \qquad (4)$$

where the function to be transformed, $g(t)$, becomes a function of both position t_0 and scale λ. The wavelet ψ (ψ^* is its conjugate) behaves as a mathematical microscope, with magnification λ^{-1} and point of focus x_0. The exponent r can be chosen so that either wavelet energy is conserved ($r = 2$) or wavelet magnitude is conserved ($r = 1$). In the present work, the u component of velocity is transformed with $r = 1$, so that the wavelet coefficients have units of velocity, too. The wavelet transform is, therefore, ideal for separating effects at different scales, in this case, the effects of flapping from those of the large eddies.

Here the real Mexican hat (or Marr) wavelet is used and is defined by

$$\psi(t) = (1 - t^2)e^{-t^2/2} \qquad (5)$$

In Fig. 10, the dilatation (scale) is normalized as $\lambda U_e/x_R$. The scale λ is twice the length of time between zero crossings of the wavelet so that it corresponds to the period of a sine wave used in the Fourier analysis for the spectra in Figs. 5 and 6. In the impermeable case, two scales dominate: the first between $\lambda u_e/x_R = 10$ and 20, corresponding to the flapping motion, and another around $\lambda u_e/x_R = 2$, corresponding to the large eddies of the mixing layer. The 0–12.5h case shows a marked reduction in coefficient levels at scales associated with the flapping scale at $\lambda u_e/x_R = 2$ and a more regular sequence of maxima and minima. This demonstrates that the effects of the permeable surface on the fluctuating wall pressure are also present in the shear layer itself. Equivalent plots for u-component time histories measured at $x/h = 1.0$ and $y/h = -0.9$ (Figs. 10c and 10d) display the attenuating effects of the permeable surface

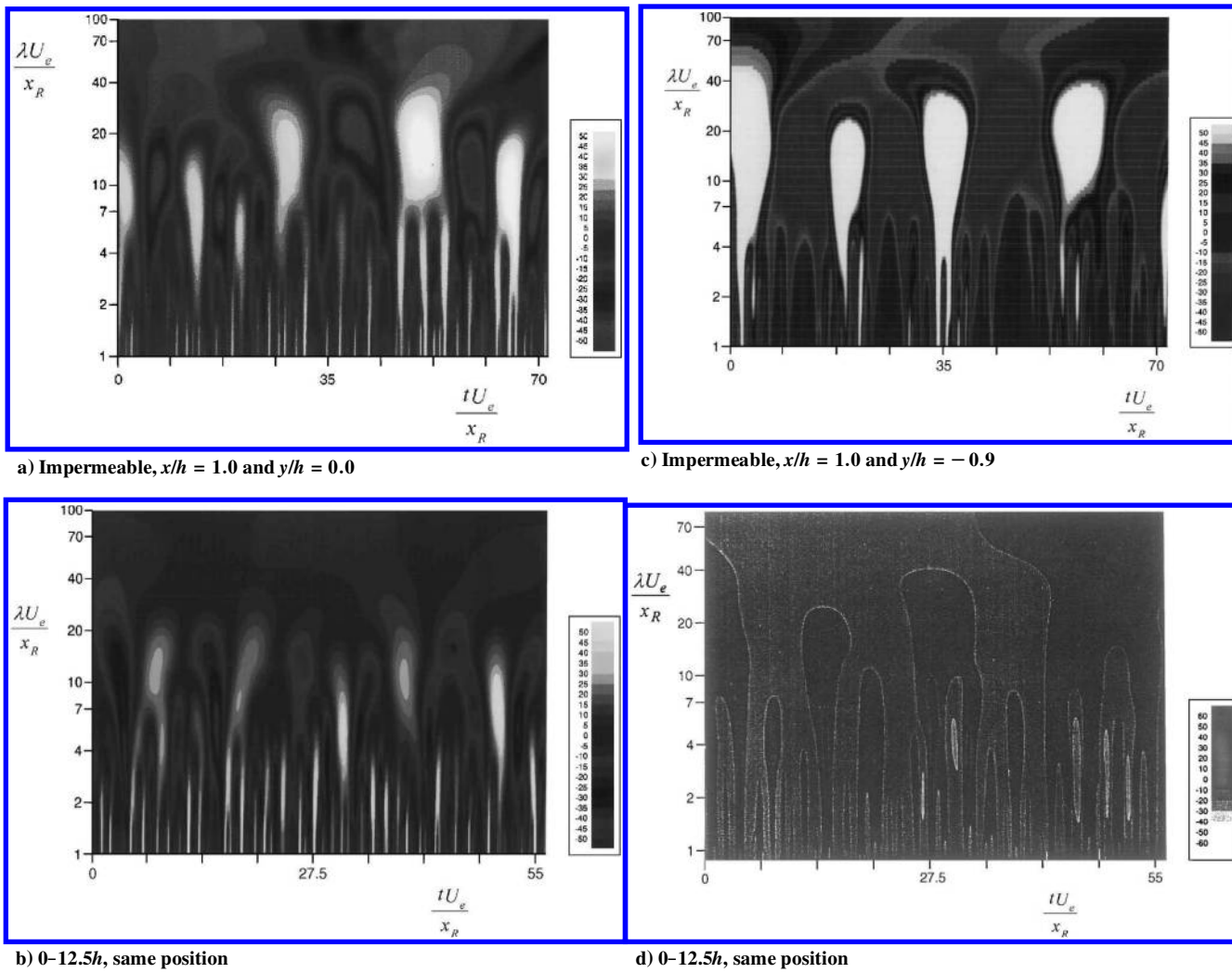

a) Impermeable, $x/h = 1.0$ and $y/h = 0.0$

c) Impermeable, $x/h = 1.0$ and $y/h = -0.9$

b) 0–12.5h, same position

d) 0–12.5h, same position

Fig. 10 Contour plots of wavelet coefficients, $\tilde{f}$.

much more graphically. The features around $\lambda = 10$–20, which are prominent in the impermeable configuration plot, are almost completely absent in the 0–12.5h permeable case.

These plots from the recirculation region also provide clues to the physical nature of the flapping process. The differences between the shapes of the peaks and troughs of the wavelet coefficients imply that the flapping is not a symmetrical process. The positive peaks, which correspond to upstream fluid motion, have an inverted droplet shape and are associated with intense events of smaller scale, probably the occasional upstream convection of a structure from the reattaching shear layer. There are no similar associations for the negative peaks, which correspond to the downstream phase of the flapping. The permeable configuration provides a continuous route for the upstream convection of fluid into the recirculation region to balance the entrainment of fluid by the shear layer out of the recirculation region, and consequently, there are few discrete instances of intense upstream convection and the resultant flapping is greatly attenuated.

Conclusions

The effect of the permeable reattachment surface (0–12.5h) is to move the peak rms wall-pressure fluctuation downstream by about 0.5h for 5% OAR and by about 2h for 20 and 50% OAR. Consistent with this, the peak rms pressure is attenuated by about 13% for the 0–12.5h, 20% OAR configuration. The drag associated with the step model is reduced by about 5%, although this figure can be increased to about 9% by reducing the streamwise length of the permeable section to only 3.5h.

The peak flapping frequency at $n \approx 0.1$ reaches a maximum at $x/h = 4.5$ for the impermeable case, and this position coincides with that of maximum pressure recovery in the bubble. The permeable surface appears to inhibit upstream convection of low-frequency pressure fluctuations, and this appears to be the mechanism by which the whole bubble is steadied. There is also a secondary effect as exemplified by the success of the 0–3.5h configuration in which pressure disturbances are attenuated by the permeable surface, and this is the main reason for the structural changes that occur upstream of reattachment and for $n > 2$, approximately. These changes are not evident downstream of reattachment as the spectra there collapse reliably on the variables U_e and x_R.

Acknowledgments

This work is jointly supported under Grant GR/J 14844 by the Engineering and Physical Sciences Research Council and the Ministry of Defence. The wavelet analysis was carried out as part of a collaborative agreement with support from British Council Undergrant ROM/889/94/127. We are also grateful to D. G. Mabey for suggesting the work originally and for his continuing support and interest.

References

[1] Mabey, D. G., "Analysis and Correlation of Data on Pressure Fluctuations in Separated Flow," *Journal of Aircraft*, Vol. 9, No. 9, 1972, pp. 642–645.

[2] Wood, D. H., and Bradshaw, P., "A Turbulent Mixing Layer Constrained by a Solid Surface. Part 1. Measurements Before Reaching the Surface," *Journal of Fluid Mechanics*, Vol. 122, 1982, pp. 57–89.

[3] Kim, J., "On the Structure of Pressure Fluctuations in Simulated Turbulent Channel Flow," *Journal of Fluid Mechanics*, Vol. 205, 1989, pp. 421–451.

[4] Farabee, T. M., and Casarella, M. J., "Measurements of Fluctuating Wall Pressure for Separated/Reattached Boundary Layer Flows," *Journal of*

Vibration, Acoustics, Stress and Reliability in Design, Vol. 108, 1986, pp. 301–307.

[5]Simpson, R. L., "Turbulent Boundary Layer Separation," *Annual Review of Fluid Mechanics*, Vol. 21, 1989, pp. 205–234.

[6]Driver, D. M., Seegmiller, H. L., and Marvin, J. G., "Time-Dependent Behavior of a Reattaching Shear Layer," *AIAA Journal*, Vol. 25, No. 7, 1987, pp. 914–919.

[7]Cherry, N. J., Hillier, R., and Latour, M. E. M. P., "Unsteady Measurements in a Separated and Reattaching Flow," *Journal of Fluid Mechanics*, Vol. 144, 1984, pp. 13–46.

[8]Eaton, J. K., and Johnston, J. P., "Low Frequency Unsteadiness of a Reattaching Turbulent Shear Layer," *Turbulent Shear Flows 3*, edited by L. J. S. Bradbury, F. Durst, B. E. Launder, F. W. Schmidt, and J. H. Whitelaw, Springer–Verlag, Berlin, 1982, pp.162–170.

[9]Castro, I. P., and Haque, A., "The Structure of a Turbulent Shear Layer Bounding a Separation Region," *Journal of Fluid Mechanics*, Vol. 179, 1987, pp. 439–468.

[10]Kiya, M., and Sasaki, K., "Structure of a Turbulent Separation Bubble," *Journal of Fluid Mechanics*, Vol. 137, 1983, pp. 83–113.

[11]Kiya, M., and Sasaki, K., "Structure of Large-Scale Vortices and Unsteady Reverse Flow in the Reattaching Zone of a Turbulent Separation Bubble," *Journal of Fluid Mechanics*, Vol. 154, 1985, pp. 463–491.

[12]Chandrsuda, C., and Bradshaw, P., "Turbulence Structure of a Reattaching Mixing Layer," *Journal of Fluid Mechanics*, Vol. 110, 1981, pp. 171–194.

[13]Ruderich, R., and Fernholz, H. H., "An Experimental Investigation of a Turbulent Shear Flow with Separation, Reverse Flow, and Reattachment," *Journal of Fluid Mechanics*, Vol. 163, 1986, pp. 283–322.

[14]Bradshaw, P., and Wong, F. Y. F., "The Reattachment and Relaxation of a Turbulent Shear Layer-Wall," *Journal of Fluid Mechanics*, Vol. 52, Pt. 1, 1972, pp. 113–135.

[15]Rockwell, D., "Oscillations of Impinging Shear Layers," *AIAA Journal*, Vol. 21, No. 5, 1983, pp. 645–664.

[16]Rockwell, D., and Naudascher, E., "Self-Sustained Oscillations of Impinging Free Shear Layers," *Annual Review of Fluid Mechanics*, Vol. 11, 1979, pp. 67–94.

[17]de Brederode, V. A. S. L., and Bradshaw, P., "Three-Dimensional Flow in Nominally Two-Dimensional Separation Bubbles I. Flow Behind a Rearward-Facing Step," Dept. of Aeronautics, Rept. 72-19, Imperial College, London, 1972.

[18]Morrison, J. F., and Bradshaw, P.,"Bursts and Wall-Pressure Fluctuations in Turbulent Boundary Layers" (manuscript in preparation).

[19]Owen, T. B., "Techniques of Pressure-Fluctuation Measurements Employed in the RAE Low-Speed Wind-Tunnels," AGARD Rept. 172, 1958.

[20]Horne, M. P., and Handler, R. A., "Note on the Cancellation of Contaminating Noise in the Measurement of Turbulent Wall Pressure Fluctuations," *Experiments in Fluids*, Vol. 12, 1991, pp. 136–139.

[21]Le, H., and Moin, P., "Direct Numerical Simulation of Turbulent Flow over a Backward Facing Step," Dept. of Mechanical Engineering, Rept. TF-58, Stanford Univ., Stanford, CA, 1994.

[22]Devenport, W. J., and Sutton, E. P., "Near-Wall Behavior of Separated and Reattaching Flows," *AIAA Journal*, Vol. 29, No. 1, 1991, pp. 25–31.

[23]Heenan, A. F., and Morrison, J. F., "Passive Control of Backstep Flow," *Experimental and Thermal Fluid Science* (to be published).

[24]Heenan, A. F., and Morrison, J. F., "Triple-Split Fibre-Film Probes for Reversing Flows," *Measurement Science Technology* (to be published).

[25]Daubechies, I., *Ten Lectures on Wavelets*, Conf. Board of the Mathematical Sciences, National Science Foundation, Regional Conf. Series in Applied Mathematics, 1992.

D. Parekh
Associate Editor

This article has been cited by:

1. Phillip J. Ansell, Michael BraggCharacterization of Ice-Induced Low-Frequency Flowfield Oscillations and their Effect on Airfoil Performance . [Citation] [PDF] [PDF Plus]
2. Grégoire Fourrié, Laurent Keirsbulck, Larbi Labraga. 2013. Wall shear stress characterization of a 3D bluff-body separated flow. *Journal of Fluids and Structures* . [CrossRef]
3. Jeremy A. Dahan, A. S. Morgans, S. Lardeau. 2012. Feedback control for form-drag reduction on a bluff body with a blunt trailing edge. *Journal of Fluid Mechanics* **704**, 360-387. [CrossRef]
4. W. A. El-Askary, M. El-Mayet, A. Balabel. 2012. On the performance of sudden-expansion pipe without/with cross-flow injection: experimental and numerical studies. *International Journal for Numerical Methods in Fluids* **69**:2, 366-383. [CrossRef]
5. Ryan Gerakopulos, Serhiy Yaruseyvich. 2012. Novel Time-Resolved Pressure Measurements on an Airfoil at a Low Reynolds Number. *AIAA Journal* **50**:5, 1189-1200. [Citation] [PDF] [PDF Plus]
6. Minsuk Ji, Meng Wang. 2012. Surface pressure fluctuations on steps immersed in turbulent boundary layers. *Journal of Fluid Mechanics* **712**, 471. [CrossRef]
7. V. I. Terekhov, Ya. I. Smulskii, K. A. Sharov. 2012. Interference of separated flows behind backward-facing step in the presence of passive control. *Technical Physics Letters* **38**:2, 125. [CrossRef]
8. Serhiy Yarusevych, Ryan GerakopulosNovel Time-Resolved Pressure Measurements on an Airfoil at Low Reynolds Numbers . [Citation] [PDF] [PDF Plus]
9. Pierre-Elie Weiss, Sébastien Deck. 2011. Control of the antisymmetric mode (m = 1) for high Reynolds axisymmetric turbulent separating#reattaching flows. *Physics of Fluids* **23**:9, 095102. [CrossRef]
10. Jae-Eun Cha, Hyoung-Woo Kim, Hyoung-Bum Kim. 2010. Experimental Investigation of Two-dimensionality of Flow around the Vertical Fence Submerged in a Turbulent Boundary Layer. *Journal of the Korean Society of Visualization* **8**:1, 13-18. [CrossRef]
11. Nan Gao, Dan EwingInvestigation of Large Scale Flow Structures in an Offset Attaching Jet Using Spectral Linear Stochastic Estimation . [Citation] [PDF] [PDF Plus]
12. Antonius Aditjandra, Barry J. Trosin, Ahmed M. Naguib. 2009. Array measurements of the surface pressure beneath a forced axi-symmetric separation bubble. *Experiments in Fluids* **46**:2, 297. [CrossRef]
13. Y. Li, A. M. Naguib, L. M. Hudy. 2008. Two-Point Measurements of Wall Shear Stress Beneath an Axisymmetric Separating/Reattaching Flow. *AIAA Journal* **46**:10, 2649-2652. [Citation] [PDF] [PDF Plus]
14. William Humphreys, William CullitonAn Autonomous Sensor System Architecture for Active Flow and Noise Control Feedback . [Citation] [PDF] [PDF Plus]
15. Y.Z. Liu, F. Ke, H.J. Sung. 2008. Unsteady separated and reattaching turbulent flow over a two-dimensional square rib. *Journal of Fluids and Structures* **24**:3, 366. [CrossRef]
16. Franck Simon, Sébastien Deck, Philippe Guillen, Roxan Cayzac, Alain Merlen. 2007. Zonal-Detached-Eddy Simulation of Projectiles in the Subsonic and Transonic Regimes. *AIAA Journal* **45**:7, 1606-1619. [Citation] [PDF] [PDF Plus]
17. Nan Gao, Dan Ewing. 2007. Experimental investigation of planar offset attaching jets with small offset distances. *Experiments in Fluids* **42**:6, 941. [CrossRef]
18. Sebastien Deck, Pascal Thorigny. 2007. Unsteadiness of an axisymmetric separating-reattaching flow: Numerical investigation. *Physics of Fluids* **19**:6, 065103. [CrossRef]
19. Laura M. Hudy, Ahmed Naguib, William M. Humphreys. 2007. Stochastic estimation of a separated-flow field using wall-pressure-array measurements. *Physics of Fluids* **19**:2, 024103. [CrossRef]
20. Sarah Blackmar, Richard HillierUnsteady Properties of a Separated and Reattaching Flow . [Citation] [PDF] [PDF Plus]
21. Nan Gao, Dan EwingInvestigation of the Large Scale Flow Structures in Dual Planar Attaching Jets . [Citation] [PDF] [PDF Plus]
22. Nan Gao, Jonathan Naughton, Dan EwingMeasurements of wall shear stress of an offset attaching planar jet with co-flow . [Citation] [PDF] [PDF Plus]
23. Ibrahim Elrayah Abdalla, Zhiyin Yang. 2005. Numerical Study of a Separated-Reattached Flow on a Blunt Plate. *AIAA Journal* **43**:12, 2465-2474. [Citation] [PDF] [PDF Plus]

24. Yongxiang Li, Ahmed M. Naguib. 2005. High-Frequency Oscillating-Hot-Wire Sensor for Near-Wall Diagnostics in Separated Flows. *AIAA Journal* **43**:3, 520-529. [Citation] [PDF] [PDF Plus]
25. Nan Gao, Dan Ewing. 2005. Investigation of the Large-Scale Flow Structures in the Cooling Jets Used in the Blown Film Manufacturing Process. *Journal of Fluids Engineering* **127**:5, 978. [CrossRef]
26. Yongxiang Li, Ahmed NaguibA High-Frequency Oscillating-Hot-Wire Sensor for Near-Wall Diagnostics in Separated Flows . [Citation] [PDF] [PDF Plus]
27. Laura M. Hudy, Ahmed M. Naguib, William M. Humphreys. 2003. Wall-pressure-array measurements beneath a separating/reattaching flow region. *Physics of Fluids* **15**:3, 706. [CrossRef]
28. 2002. Study on the Passive Shock/Boundary Layer Interaction Control in Transonic Moist Air Flow. *Journal of the Korean Society for Aeronautical Space Science* **30**:8, 21-29. [CrossRef]
29. Pier Giorgio Spazzini. 2002. Effects of calibration data reduction on a probe performance. *Measurement Science and Technology* **13**:9, 1404-1413. [CrossRef]
30. Avi Seifert, Latunia G. Pack. 2002. Active Flow Separation Control on Wall-Mounted Hump at High Reynolds Numbers. *AIAA Journal* **40**:7, 1363-1372. [Citation] [PDF] [PDF Plus]
31. G. A. Flynn, J. F. Morrison, D. G. Mabey. 2001. Buffet Alleviation on Swept and Unswept Wings at High Incidence. *Journal of Aircraft* **38**:2, 368-378. [Citation] [PDF] [PDF Plus]
32. Charles-Henri Bruneau, Iraj Mortazavi. 2001. Contrle passif d'coulements incompressibles autour d'obstacles l'aide de milieux poreux. *Comptes Rendus de l'Acadmie des Sciences - Series IIB - Mechanics* **329**:7, 517. [CrossRef]
33. Charles-Henri Bruneau, Iraj MortazaviThe penalization method 1098-1100. [CrossRef]
34. Avi Seifert, LaTunia PackActive control of separated flows on generic configurations at high Reynolds numbers . [Citation] [PDF] [PDF Plus]
35. A F Heenan, J F Morrison. 1998. Split-film probes in recirculating flow. *Measurement Science and Technology* **9**:4, 638. [CrossRef]